Article

The Neutron Mean Life and Big Bang Nucleosynthesis

Tsung-Han Yeh [1], Keith A. Olive [2],* and Brian D. Fields [3]

[1]   TRIUMF, 4004 Wesbrook Mall, Vancouver, BC V6T 2A3, Canada
[2]   William I. Fine Theoretical Physics Institute, School of Physics and Astronomy, University of Minnesota, Minneapolis, MN 55455, USA
[3]   Department of Astronomy and of Physics, Illinois Center for Advanced Study of the Universe, University of Illinois, Urbana, IL 61801, USA
*   Correspondence: olive@umn.edu

Abstract: We explore the effect of neutron lifetime and its uncertainty on standard big bang nucleosynthesis (BBN). BBN describes the cosmic production of the light nuclides, ^{1}H, D, ^{3}H+^{3}He, ^{4}He, and ^{7}Li+^{7}Be, in the first minutes of cosmic time. The neutron mean life τ_n has two roles in modern BBN calculations: (1) it normalizes the matrix element for weak $n \leftrightarrow p$ interconversions, and (2) it sets the rate of free neutron decay after the weak interactions freeze-out. We review the history of the interplay between τ_n measurements and BBN, and present a study of the sensitivity of the light element abundances to the modern neutron lifetime measurements. We find that τ_n uncertainties dominate the predicted ^{4}He error budget, but these theory errors remain smaller than the uncertainties in ^{4}He observations, even with the dispersion in recent neutron lifetime measurements. For the other light element predictions, τ_n contributes negligibly to their error budget. Turning the problem around, we combine present BBN and cosmic microwave background (CMB) determinations of the cosmic baryon density to *predict* a "cosmologically preferred" mean life of $\tau_n(\text{BBN} + \text{CMB}) = 870 \pm 16$ s, which is consistent with experimental mean life determinations. We show that if future astronomical and cosmological helium observations can reach an uncertainty of $\sigma_{\text{obs}}(Y_p) = 0.001$ in the ^{4}He mass fraction Y_p, this could begin to discriminate between the mean life determinations.

Keywords: cosmology; big bang nucleosynthesis; neutron lifetime

1. Introduction

The origin of the light elements (^{1}H, D, ^{3}He, ^{4}He, and ^{7}Li) is well explained by big bang nucleosynthesis (BBN) taking place in the early Universe, when the temperature scale was roughly 1 MeV and below, i.e., the energies associated with nuclear reactions [1–9]. Because the physics of these energies is well-known, testable predictions of BBN are possible given reliable nuclear cross sections and the subject of this contribution, a well-measured neutron lifetime [10].

Standard BBN is the theoretical framework that implements these cross sections in the context of both the Standard Models of particle physics and cosmology, and is the model we will adopt for this paper. For cosmology, we will thus assume ΛCDM. For BBN, this means that the Universe was dominated by photon and neutrino radiation during BBN, with a baryon density consistent with that determined from measurements of the cosmic microwave background (CMB) anisotropies [11]; it is useful to parameterize the baryon density in terms of baryon-to-photon ratio $\eta \equiv n_{\text{b}}/n_\gamma$, with the density of blackbody photons fixed by the temperature: $n_\gamma \propto T^3$. From the Standard model of electroweak interactions, we will assume that the number of light neutrino flavors is $N_\nu = 3$ and that there are no other relativistic contributions to the energy density.

Historically, progress in BBN has been tightly linked to progress in the measurement of the neutron lifetime. Until the 1980s, the uncertainties in the prediction of the light element abundances by BBN were dominated by the uncertainty of these three parameters

(η, N_ν, τ_n); this was prior to the CMB determination of the baryon density, the measurement of the number of neutrino flavors at LEP/SLAC [12], and the vast improvement in the measurement of the neutron lifetime [13,14]. For example, the primordial helium mass fraction is sensitive to the variation in each of these quantities, as can be seen in Figure 1 taken from the 1981 analysis in Ref. [13]. In this figure, the helium mass fraction, $Y_p = \rho(^4\text{He})/\rho_{\text{baryon}}$ is plotted as a function of the baryon-to-photon ratio η for three values of N_ν and three values for the neutron lifetime[1]. At the time, BBN provided the best estimate for η and N_ν (this was pre-LEP/SLAC and direct limits from accelerators on N_ν were quite poor [15]). The values of τ_n used here corresponded to what was the "accepted" value for the neutron half-life, $\tau_{1/2} = 10.61 \pm 0.16$ min corresponding to a mean life $\tau_n = 918 \pm 14$ s that came from a 1972 paper by Christensen et al. [16]; and more recent though very different determinations of $\tau_{1/2} = 10.13 \pm 0.09$ min or $\tau_n = 877 \pm 8$ s by Bondarenko et al. [17]; and $\tau_{1/2} = 10.82 \pm 0.20$ min or $\tau_n = 937 \pm 17$ s [18] by Byrne et al.
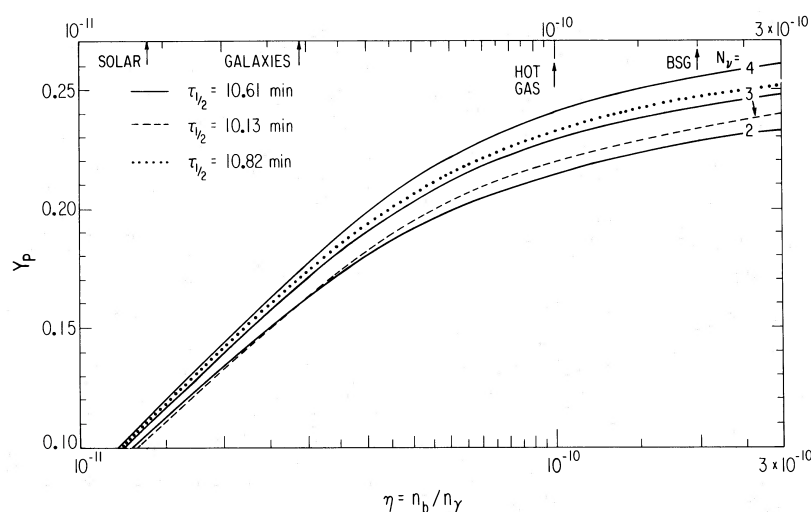
Figure 1. The helium mass fraction as a function of the baryon-to-photon ratio for three choices of $N_\nu = 2, 3$, and 4 and three choices of $\tau_{1/2}$ with $N_\nu = 3$. Figure circa 1981 from ref. [13].

It is also interesting to note the range in η shown in this 1981 figure. It spans values of η from 10^{-11} (corresponding to mass-to-light ratios typical of the solar neighborhood) to 3×10^{-10}. Today, η is quite well determined [8,9,19]: $\eta_{10} = 10^{10}\eta = 6.104 \pm 0.055$ from CMB data alone [11], and $\eta_{10} = 6.115 \pm 0.038$ from a combination of BBN, CMB and light element abundance observations. Clearly, our understanding of the baryon density of the Universe has progressed.

The Review of Particle Properties in 1982 [20] quoted an average neutron mean life of $\tau_n = 925 \pm 11$ s based on the Christensen et al. and Byrne et al. measurements along with a measurement by Kosvintsev et al. [21], which gave $\tau_n = 875 \pm 95$ s. The Bondarenko et al. measurement was excluded as it was "in significant disagreement with the other two precise direct mean life measurements and the inferred value given by Wilkinson 80" [22]. In the 1984 edition of the Review of Particle Properties [23], the Bondarenko measurement was included replacing Kosvintsev 1980 giving $\tau_n = 898 \pm 16$ s, noting that the origin of the discrepancies between the measurements was not known. Because of the discrepancies, the uncertainty in the mean was inflated by a scale factor of 2.4.

It was not until 1990 that Mampe et al. [24] presented a significantly more accurate result $\tau_n = 887.6 \pm 3.0$ s using ultra cold neutrons in a fluid-walled bottle. This had a strong effect on the world average, which was now 888.6 ± 3.5, based on seven measurements. The discrepancy was largely gone, and the scale factor for the uncertainty was reduced to 1.3, in part due to the withdrawal of the 1980 measurement by Byrne et al.

The evolution of the world average is plotted in Figure 2, showing the average mean lifetime since 1960. These values are collected in Table 1, which only shows years in

which the average mean life changed. Here, multiple uncertainties have been combined in quadrature. One clearly sees the marked drop in the value and uncertainty following the Mampe et al. measurement. The impact of this measurement on BBN was immediate [25] since, as described in more detail below, the uncertainty in the predicted helium abundance is very sensitive to the uncertainty in the neutron mean lifetime [26],

$$\frac{\Delta Y_p}{Y_p} \simeq 0.730 \frac{\Delta \tau_n}{\tau_n} \,, \tag{1}$$

meaning that a drop in the uncertainty from 16 to 3.5 reduced the uncertainty in Y_P from 0.0032 to 0.0007, assuming $Y_p = 0.247$.
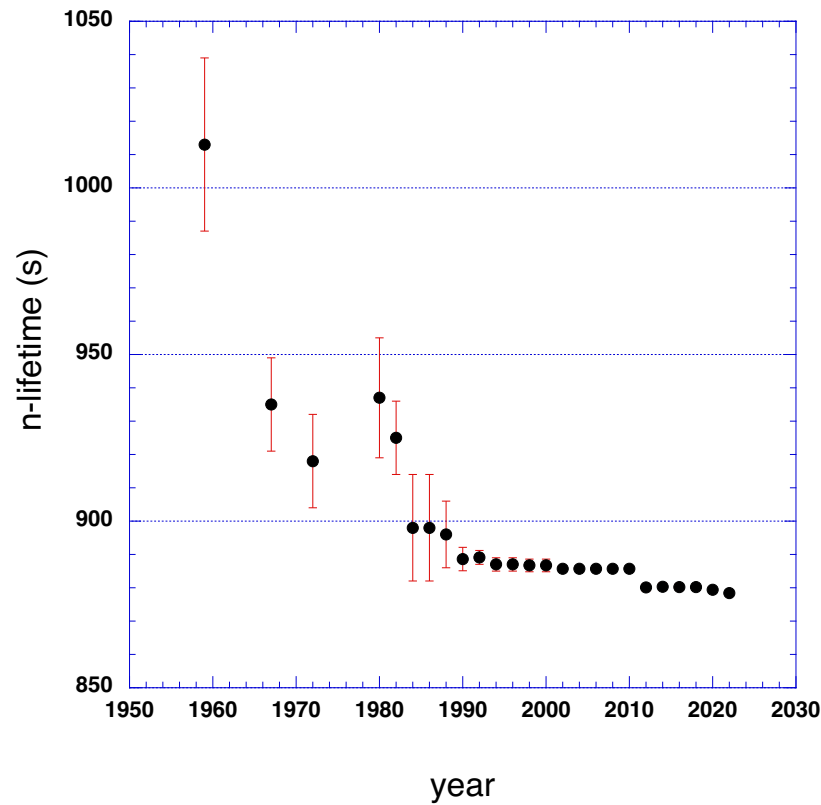
Figure 2. The average mean lifetime of the neutron as compiled by the Review of Particle Properties/Physics. Please note that the uncertainty in the mean life for more recent measurements is smaller than the symbol showing the mean.

Table 1. Neutron mean life and uncertainty (in s) as reported by the review of Particle Properties and Review of Particle Physics.

Year	τ_n	σ_{τ_n}	Year	τ_n	σ_{τ_n}	Year	τ_n	σ_{τ_n}
1959	1013	± 26	1967	935	± 14	1972	918	± 14
1980	937	± 18	1982	925	± 11	1984	898	± 16
1988	896	± 10	1990	888.6	± 3.5	1992	889.1	± 2.1
1994	887.0	± 2.0	1998	886.7	± 1.9	2002	885.7	± 0.8
2012	880.1	± 1.1	2014	880.3	± 1.1	2016	880.2	± 1.0
2020	879.4	± 0.6	2022	878.4	± 0.5			

By the time of the 2002 edition of the Review of Particle Physics [27], there were enough high-quality direct measurements allowing the Particle Data Group (PDG) to drop measurements with uncertainties larger than 10 s. This led to another impressive drop in the uncertainty of the mean, with $\tau_n = 885.7 \pm 0.8$ s. This drop was largely driven by the

measurement of Arzumanov et al. [28] and further dropped the uncertainty in Y_P to 0.0002, making the dominant source of uncertainty (at the time) other nuclear rates [29].

At about this time, WMAP provided the first all-sky measurements of anisotropies in the CMB temperature [30]. These fluctuations encode a wealth of cosmological parameters, including the baryon density or baryon-to-photon ratio η. Using this input from the CMB along with the improvements in the measurements of τ_n effectively made BBN a parameter-free theory [31].

However, it is certainly reasonable to question whether the quoted uncertainties are truly reflective of the systematic errors included. In 2005, Serebrov et al. [32] published a result which was in fact systematically lower than the previous world average, $\tau_n = 878.5 \pm 0.7 \pm 0.3$. This value was used in a BBN analysis in Ref. [33]. As a sole and severely discrepant value, it was not included in the PDG average until 2012 [34] when additional low values were reported. The 2012 average was now $\tau_n = 880.1 \pm 1.1$ where the uncertainty has been scaled by a factor of 1.8. This seismic shift in τ_n is clearly seen in Figure 2. An ideogram of the seven measurements leading to this average is shown in Figure 3a[2]. Here, we see the onset of a discrepancy in τ_n. The vertical blue rectangle corresponds to the 2012 mean and 1σ spread. A review including a discussion of the methods used to obtain τ_n can be found in [35].

(**a**)　　　　　　　　　　　　　　　　　　　　　　　　　　(**b**)
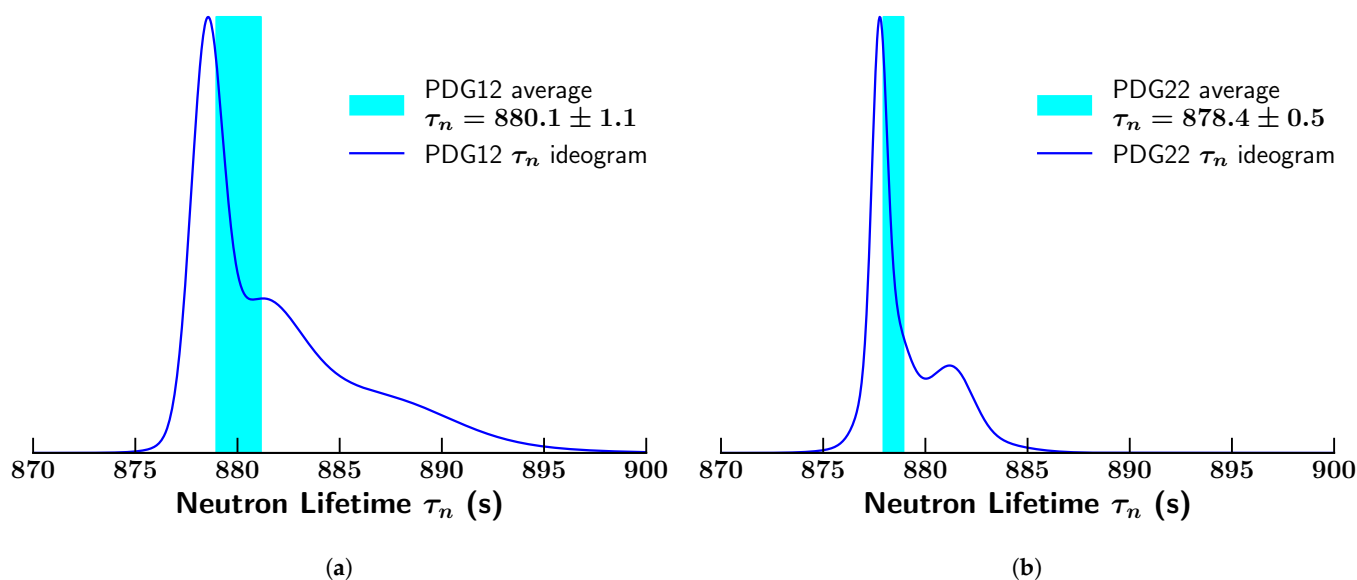
Figure 3. Ideograms for neutron lifetime measurements. (**a**) Ideogram for the seven measurements contributing to the PDG average neutron mean life in 2012; (**b**) Ideogram for the eight measurements contributing to the PDG average neutron mean life in 2022.

Subsequent changes in the world average have been relatively minor—certainly from the perspective of BBN calculations [19], where the current value of

$$\tau_n = 878.4 \pm 0.5 \text{ s} \tag{2}$$

based on eight measurements [10,32,36–42] is used. As the uncertainties in individual measurements continue to drop, the discrepancy appears more pronounced, and the uncertainty already includes a scale factor of 1.8 [10]. This can be seen in the current ideogram shown in Figure 3b.

Despite the tightness of the world average in Equation (2), the neutron lifetime remains an outstanding puzzle. The results used in Equation (2) are based on confined ultracold neutrons, with earlier experiments using material bottles, and later experiments using magnetic and gravitational traps. The measurements in traps give consistent results, with recent very precise UCNτ determination [42] dominating the weighted averages among them and

leading to the sharp peak in Figure 3b. The most recent bottle measurements give lifetimes systematically longer than the trap measurements, leading to the shoulder to the right of the peak in Figure 3b. The resulting *dispersion* between the trap and bottle measurements is of order $\Delta\tau_n \sim 5$ s, and could stem from systematic differences between the methods. There is, in addition, an in-beam measurement by Yue et al. [43] with a relatively high value of $\tau_n = 887.7 \pm 1.2 \pm 1.9$ s. This differs from the best trap measurement by $\Delta\tau_n \sim 10$ s. We will not here enter further into the current discrepancies, noting only that for a recent discussion of the differences between the ultracold neutron results (the ones used in the PDG average) and the in-beam results, the reader should see [44] as well as other articles in this Special Issue.

In what follows, we will first briefly review the role of the neutron lifetime in standard BBN calculations in Section 2. We will also review the current results of BBN based on the latest input nuclear cross-sections (including τ_n) and abundance data. In Section 3, we will discuss the sensitivity of the results to τ_n. We will also test the potential effect of the τ_n discrepancy instead of Monte Carlo sampling of the Gaussian corresponding to the mean value of τ_n (and its uncertainty), but as a test, we will use the ideogram in Figure 3b to sample values of τ_n—keeping in mind that this procedure is not fully rigorous. In Section 4, we will take a novel approach to τ_n and treat it again as a parameter for which we generate a likelihood function and make a BBN prediction for τ_n. Finally, in Section 5, we summarize the current state of BBN with respect to the neutron lifetime.

2. Standard BBN

Standard BBN (SBBN) is built upon Standard Model of nuclear and particle physics, in the background of the Friedmann-Robertson-Walker cosmological model based on Einstein gravity. We assume only the standard set of nuclear and particle interactions and nuclear and particle content[3], in particular, with $N_\nu = 3$. Furthermore, in SBBN, we assume a radiation-dominated Universe during the epoch of nucleosynthesis. The radiation density can be expressed as
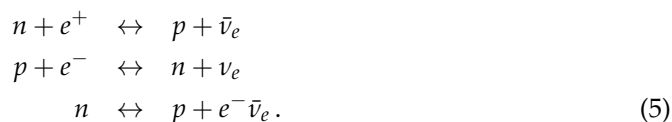
$$\rho = \frac{\pi^2}{30}\left(2 + \frac{7}{2} + \frac{7}{4}N_\nu\right)T^4, \tag{3}$$

taking into account the contributions of photons, electrons and positrons, and neutrino flavors appropriate for temperatures $T > 1$ MeV. The expansion rate of the Universe is determined by the Hubble parameter which can be expressed as

$$H^2 = \frac{8\pi}{3}G_N\rho, \tag{4}$$

where G_N is Newton's constant and scales as $H \propto G_N^{1/2}T^2$ in a radiation dominated universe.

The cosmic evolution of the light nuclides is plotted in Figure 4; many critical features can be understood analytically, as we now summarize. At temperatures $T \gtrsim 1$ MeV, weak interactions between neutrons and protons maintain equilibrium. These are:

$$\begin{aligned}
n + e^+ &\leftrightarrow p + \bar{\nu}_e \\
p + e^- &\leftrightarrow n + \nu_e \\
n &\leftrightarrow p + e^-\bar{\nu}_e.
\end{aligned} \tag{5}$$

As one might expect, the weak interaction rates scale as $\Gamma_{wk} \propto G_F^2 T^5$, where G_F is the Fermi constant. These reactions freeze-out when their interaction rates become slower than the expansion rate of the Universe determined by the Hubble parameter, or in other words, when the mean time between interactions is longer than the age of the Universe, determined by H^{-1}. Thus, the freeze-out condition is set by

$$G_F^2 T^5 \sim \Gamma_{wk}(T_f) = H(T_f) \sim G_N^{1/2}T^2. \tag{6}$$
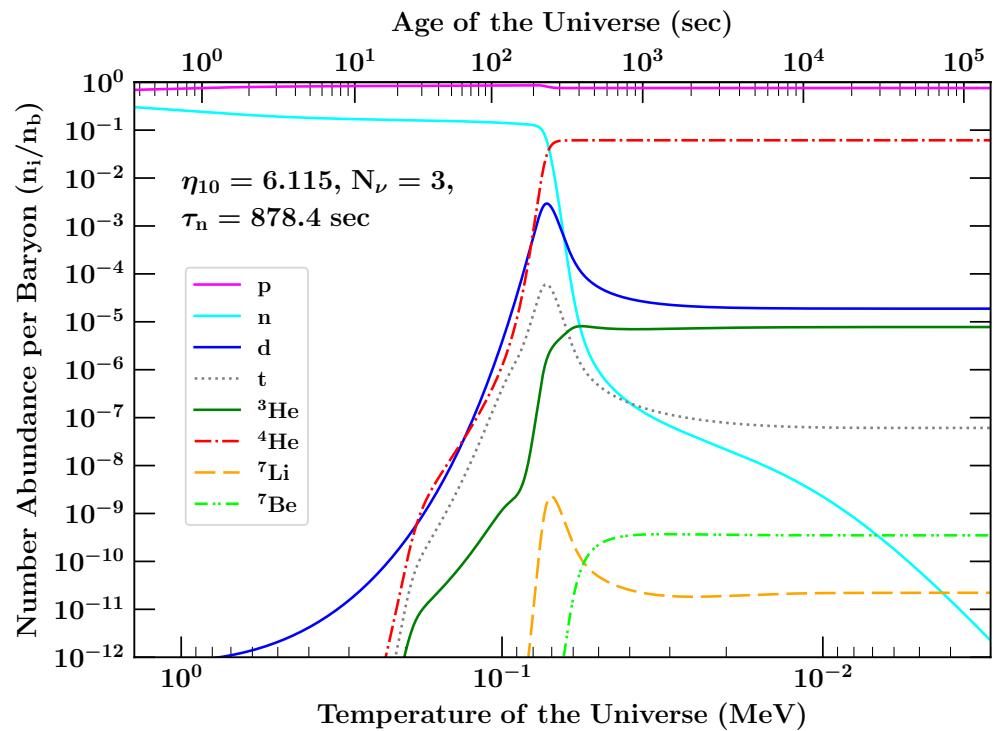
Figure 4. Time evolution of the light element abundances during BBN. Please note that time (upper axis) increases to the right, and so the temperature is shown to decrease to the right.

Weak freeze-out occurs at $T_f \simeq 0.84$ MeV, and corresponds to a flattening of the neutron and proton curves in Figure 4. At freeze-out, the neutron-to-proton ratio is given approximately by the Boltzmann factor, $(n/p)_f \simeq e^{-\Delta m/T_f} \sim 1/4.66$, where $\Delta m = m_n - m_p = 1.293$ MeV is the neutron–proton mass difference. The resulting mass fraction of neutrons at freezeout is thus $X_{n,f} = n/(n+p)|_f = (n/p)_f/[1+(n/p)_f]$.

After freeze-out, free neutron decays reduce the ratio slightly, which leads to the shallow slope in the neutron and proton curves in Figure 4. Accounting for these decays, $X_{n,\text{BBN}} = X_{n,f} e^{-t_{\text{BBN}}/\tau_n} \simeq [n/(n+p)]_f e^{-t_{\text{BBN}}/\tau_n}$ before nucleosynthesis begins at time t_{BBN}. For $t_{\text{BBN}} = 322$ s determined by the time when the photo-destruction rates of deuterium freeze-out, and $\tau_n = 878.4$ s, we have $X_{n,\text{BBN}} = 1/8.17$ or $(n/p)_{\text{BBN}} = 1/7.17$. A useful and more elaborate semi-analytic description of freeze-out can be found in [48–50].

At t_{BBN}, nucleosynthesis activity reaches a crescendo. Deuterons are formed via $np \rightarrow d\gamma$, and then undergo a series of strong reactions culminating in ^{4}He production. These rapid reactions lead to a dramatic drop in the free n abundance, as seen in Figure 4. Finally, the strong reactions also freeze-out, largely due to the inability to overcome the Coulomb barrier in the expanding and cooling plasma. Then the stable nuclides plateau, while the radioactive species ultimately decay–as shown by the free neutron decay in Figure 4 at late times.

The neutron lifetime plays two roles in BBN calculations. First, it is used to normalize the zero-temperature matrix element for weak $n - p$ interconversions (5). The rates for these reactions scale as $\Gamma_{n \leftrightarrow p} \propto 1/\tau_n$. Thus, τ_n affects the determination of the freeze-out temperature of these weak interactions. Freeze-out is determined from the competition between the weak interaction rates and the Hubble expansion as in Equation (6). Thus, an increase in the neutron lifetime leads to an increase in the freeze-out temperature leading to more neutrons at freeze-out (recall the n/p ratio scales as $e^{-\Delta m/T}$ prior to freeze-out) and hence more ^{4}He, as seen in Figures 1 and 5.
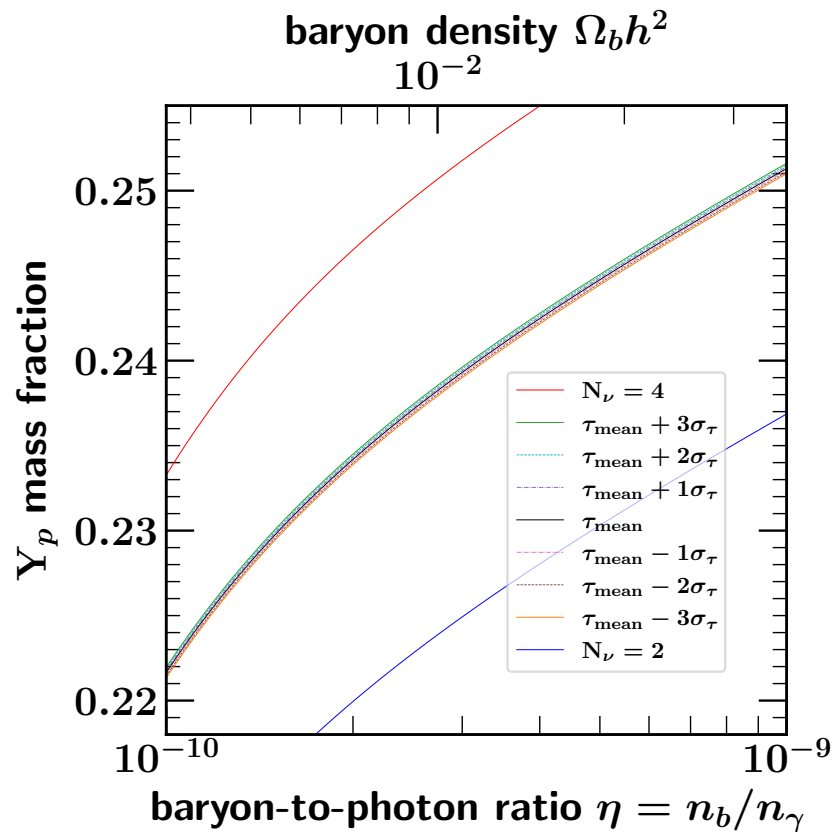
Figure 5. The helium mass fraction as a function of the baryon-to-photon ratio for three choices of $N_\nu = 2, 3$, and 4 and for a spread in values of $\tau_{1/2}$ up to $\pm 3\sigma$ about the mean with $N_\nu = 3$.

Second, the neutron lifetime controls the rate of free neutron decay, which occurs between weak freezeout at $t_f \sim 1$ s and the end of the D bottleneck at $t_d \approx 320$ s. These decays lower the n/p ratio. Therefore, an increase in the neutron lifetime leads again to more neutrons left over and hence a higher ^{4}He abundance.

Similar arguments can be made for the dependence of Y_p on N_ν and η. As one can see from Figure 5, Y_p increases with increases in all three inputs: η, N_ν, and τ_n. It is interesting to compare Figure 5 with Figure 1. Qualitatively, they are similar. However, there are several jarring differences. First, as remarked earlier, the domain in η, did not previously even cover the current best fit of $\eta_{10} = 6.115$. Second, as has been stressed in the Introduction, the relevant values of τ_n are very different. Whereas in Figure 1 values of τ_n between 877 s and 937 s, were deemed reasonable. In Figure 5, the 3σ spread in curves shown for $N_\nu = 3$, covers 876.8 s to 879.8 s. Finally, while the uncertainty in Y_p from N_ν (for $\Delta N_\nu = \pm 1$) and τ_n was comparable in Figure 1, as one can plainly see, for the same spread in N_ν, the uncertainty due a 3σ spread in τ_n is almost negligible.

3. Abundance Sensitivities to τ_n

In this section, we review the dependence of the light element abundances to τ_n. As we discussed earlier, we expect the abundance of ^{4}He to increase with increasing τ_n. It is instructive and relatively straightforward to estimate this dependence. As is well-known, the dominant isotope emerging from BBN is ^{4}He with a mass fraction of roughly 25%. In contrast, the abundance (by number) of D and ^{3}He is only of order 10^{-5}. Therefore to a good approximation, we can assume that after the deuterium bottleneck, all neutrons will eventually go to ^{4}He and we can write

$$Y_p = 2X_{n,\text{BBN}} = 2\left.\frac{n/p}{1 + n/p}\right|_{\text{BBN}} \tag{7}$$

for the ^{4}He mass fraction, where the second and third expressions are evaluated at the time t_{BBN} at the end of the deuterium bottleneck. Recalling that the neutron-to-proton ratio at freeze-out is fixed by the Boltzmann factor $e^{-\Delta m/T_{\text{f}}}$, when BBN begins, the n/p ratio is lowered by neutron decays so that

$$Y_p \;\approx\; 2(X)_{T_{\text{f}}}\, e^{-t_{\text{BBN}}/\tau_{\text{n}}} \approx 2\frac{e^{-\Delta m/T_{\text{f}}}}{1+e^{-\Delta m/T_{\text{f}}}}\, e^{-t_{\text{BBN}}/\tau_{\text{n}}} \tag{8}$$

which explicitly shows the direct τ_n dependence as well as its indirect influence through the freezeout temperature T_{f}. The latter is set by the equating the weak interaction rates $\Gamma_{np} \propto \tau_n^{-1}T^5$ and the Hubble rate $H \sim G_N^{1/2}T^2$, which gives

$$T_{\text{f}} \propto \tau_n^{1/3} \tag{9}$$

We then can trace the effect of τ_n shifts by looking at the linearized response to changes in the neutron lifetime:

$$\frac{\Delta Y_p}{Y_p} \;\approx\; \left(\frac{\partial Y_p}{\partial X}\frac{\partial X}{\partial (n/p)}\frac{\partial (n/p)}{\partial T_{\text{f}}}\frac{\partial T_{\text{f}}}{\partial \tau_n} + \frac{\partial Y_p}{\partial \tau_n}\right)\frac{\Delta \tau_n}{Y_p}. \tag{10}$$

Then using $\partial Y_p/\partial X = 2$, $\partial X/\partial (n/p) = 1/(1+n/p)^2$, $\partial (n/p)/\partial T_{\text{f}} = (n/p)\Delta m/T_{\text{f}}^2$, we can write

$$\frac{\Delta Y_p}{Y_p} \;\approx\; \left(\frac{1}{3}\frac{\Delta m}{T_{\text{f}}(1+n/p)_{\text{f}}} + \frac{t_{\text{BBN}}}{\tau_n}\right)\frac{\Delta \tau_n}{\tau_n}. \tag{11}$$

Finally using $T_{\text{f}} = 0.84$ MeV, $(n/p)_{\text{f}} = 1/4.66$, $t_{\text{BBN}} = 322$, and $\tau_n = 878.4$ s, we have

$$\frac{\Delta Y_p}{Y_p} \approx (0.42 + 0.37)\frac{\Delta \tau_n}{\tau_n} = 0.79\frac{\Delta \tau_n}{\tau_n}, \tag{12}$$

which can be compared with the full numerical dependence (at the best fit value of η) of [9] given in Equation (1). Recall that the contributions are comparable and work in the same direction: a longer τ_n leads to more ^{4}He due to (1) an earlier weak freezeout and (2) more free neutrons surviving decay.

The numerical scaling of the light element abundances to η, N_ν and τ_n, is

$$Y_p \;=\; 0.2467\left(\frac{\eta_{10}}{6.115}\right)^{0.040}\left(\frac{N_\nu}{3.0}\right)^{0.163}\left(\frac{\tau_n}{878.4 \text{ s}}\right)^{0.730}, \tag{13}$$

$$\frac{\text{D}}{\text{H}} \;=\; 2.496\times 10^{-5}\left(\frac{\eta_{10}}{6.115}\right)^{-1.634}\left(\frac{N_\nu}{3.0}\right)^{0.405}\left(\frac{\tau_n}{878.4 \text{ s}}\right)^{0.413}, \tag{14}$$

$$\frac{^3\text{He}}{\text{H}} \;=\; 1.041\times 10^{-5}\left(\frac{\eta_{10}}{6.115}\right)^{-0.570}\left(\frac{N_\nu}{3.0}\right)^{0.138}\left(\frac{\tau_n}{878.4 \text{ s}}\right)^{0.127}, \tag{15}$$

$$\frac{^7\text{Li}}{\text{H}} \;=\; 4.937\times 10^{-10}\left(\frac{\eta_{10}}{6.115}\right)^{2.117}\left(\frac{N_\nu}{3.0}\right)^{-0.285}\left(\frac{\tau_n}{878.4 \text{ s}}\right)^{0.431}, \tag{16}$$

where other inputs, such as nuclear cross-section, have been set at their mean values. These fits update those given in Ref. [26]. Please note that the exponent in Equation (13) from a numerical fit is close to the estimate in Equation (12). These fits are normalized at the Standard Model value of $N_\nu = 3$, the best fit value of $\eta_{10} = 6.115$ [19] and Equation (2) for τ_n.

The sensitivity of the ^{4}He abundance to the neutron mean life is shown in Figure 6. Typically, because the uncertainty in the neutron mean life is small, BBN predictions for the light element abundances are obtained by combining the BBN likelihood function, $\mathcal{L}_{BBN}(\eta; X_i)$, where the abundances X_i cover D, ^{3}He, ^{4}He and ^{7}Li, with a CMB likelihood function taken from Planck data [11], $\mathcal{L}_{CMB}(\eta, Y_p)$, where we include the dependence on Y_p and do not assume any a priori relation between Y_p and η [8,9]. Throughout, we are assuming $N_\nu = 3$. We can, however, include the explicit dependence on τ_n to form the following likelihood function

$$\mathcal{L}_{BBN+CMB+\tau_n}(\tau_n, X_i) \propto \int \mathcal{L}_{CMB}(\eta, Y_p)\,\mathcal{L}_{BBN}(\eta, \tau_n; X_i)\mathcal{L}_{\tau_n}(\tau_n)\,d\eta\,, \tag{17}$$

where $\mathcal{L}_{\tau_n}(\tau_n)$ can either be derived from the Gaussian with mean and uncertainty given in Equation (2) or the ideogram in Figure 3b. The projection of this likelihood function (for $X_i = Y_p$) onto the (τ_n, Y_p) plane is shown in Figure 6. Here, we show the 1, 2, and 3σ contours from a Monte Carlo scan over the neutron mean life assuming Equation (2) with a Gaussian distributed uncertainty. The star indicates the peak value of the likelihood function. The tightness of the ellipses is a consequence of the small uncertainty in τ_n. This plot is an update of that in [8]. The expected correlation between the neutron mean lifetime and ^{4}He abundance prediction is clear. It is not perfectly linear because other reaction rate uncertainties significantly contribute to the total uncertainty in ^{4}He as sampled in our Monte Carlo. These include rates for $p(n, \gamma)d$, $d(d, n)^3$He, and $d(d, p)t$. Please note that marginalizing over τ_n determines the theoretical ^{4}He likelihood function discussed below.
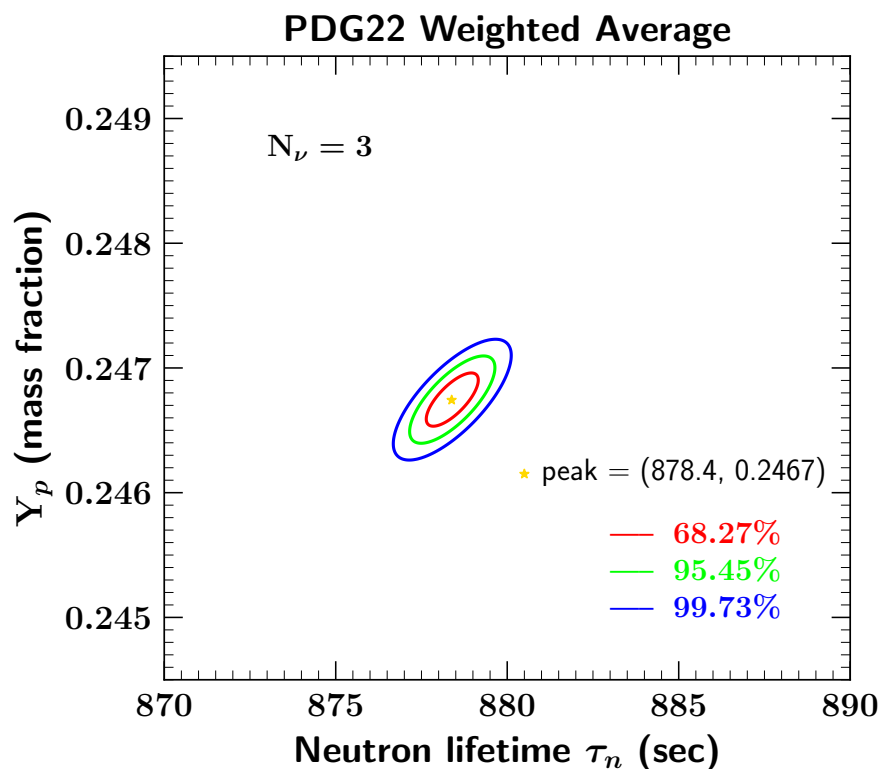
Figure 6. The sensitivity of the ^{4}He abundance to the neutron mean lifetime, assuming a Gaussian distribution for τ_n with mean and uncertainty given by Equation (2). In addition to the peak of the likelihood, denoted by a star, we show the 1, 2, and 3σ contours.

If instead of taking a Gaussian distribution with mean and uncertainty given by Equation (2), we use the distribution indicated by the ideogram in Figure 3b, we obtain the elongated prediction for Y_p shown in Figure 7. While the ideogram distribution should not be taken as statistically rigorous, we remind the reader that there is somewhat significant

dispersion in the experimental results for τ_n (a scale factor of 1.8 was already applied to obtain $\sigma_{\tau_n} = 0.5$ s) and the Gaussian may mask the true uncertainty.[4] The tail end of the ideogram has lifetimes up to about 885 s, leading to significantly more ^{4}He.

PDG22 Ideogram
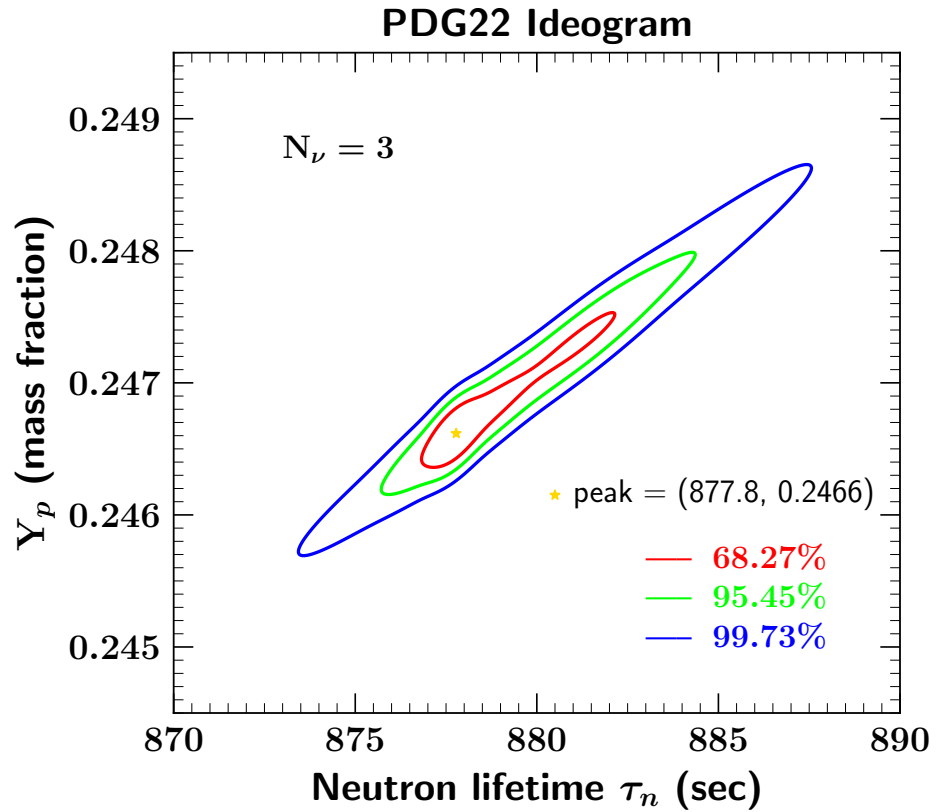
Figure 7. As in Figure 6 where we have assumed the distribution of τ_n taken from the ideogram in Figure 3b.

It is also common to compare the predictions of BBN to the observations by examining the theoretical and observational likelihood functions [8,9,26]. The theoretical likelihood function can be expressed as a convolution of the BBN theory, dependent on η (we again fix $N_\nu = 3$) and the CMB likelihood functions. The combined likelihood is defined by

$$\mathcal{L}_{\text{BBN}+\text{CMB}}(X_i) \propto \int \mathcal{L}_{\text{CMB}}(\eta, Y_p)\,\mathcal{L}_{\text{BBN}}(\eta; X_i)\,d\eta \propto \int \mathcal{L}_{\text{BBN}+\text{CMB}+\tau_n}(\tau_n, X_i)d\tau_n\,. \quad (18)$$

The second proportionality indicates that the combined BBN and CMB likelihood function is given by marginalizing Equation (17) over τ_n. We normalize each of the likelihood functions so that at their peaks $\mathcal{L} = 1$. Figure 8 shows the comparison of these likelihood functions for (a) Y_p (upper left), (b) D/H (upper right), (c) ^{3}He/H (lower left), and (d) ^{7}Li/H (lower right). In the case of ^{4}He, we show all three likelihood functions. The combined CMB-BBN likelihood from Equation (18), $\mathcal{L}_{\text{CMB}-\text{BBN}}(Y)$, is shaded purple. The observational likelihood determined from [51,52]

$$Y_{p,\text{obs}} = 0.2448 \pm 0.0033\,. \quad (19)$$

is shaded yellow. The CMB-only likelihood, given by

$$\mathcal{L}_{\text{CMB}}(Y_p) \propto \int \mathcal{L}_{\text{CMB}}(\eta, Y_p)\,d\eta\,. \quad (20)$$

is shaded cyan. Given the observational and CMB uncertainties, the agreement is quite good.
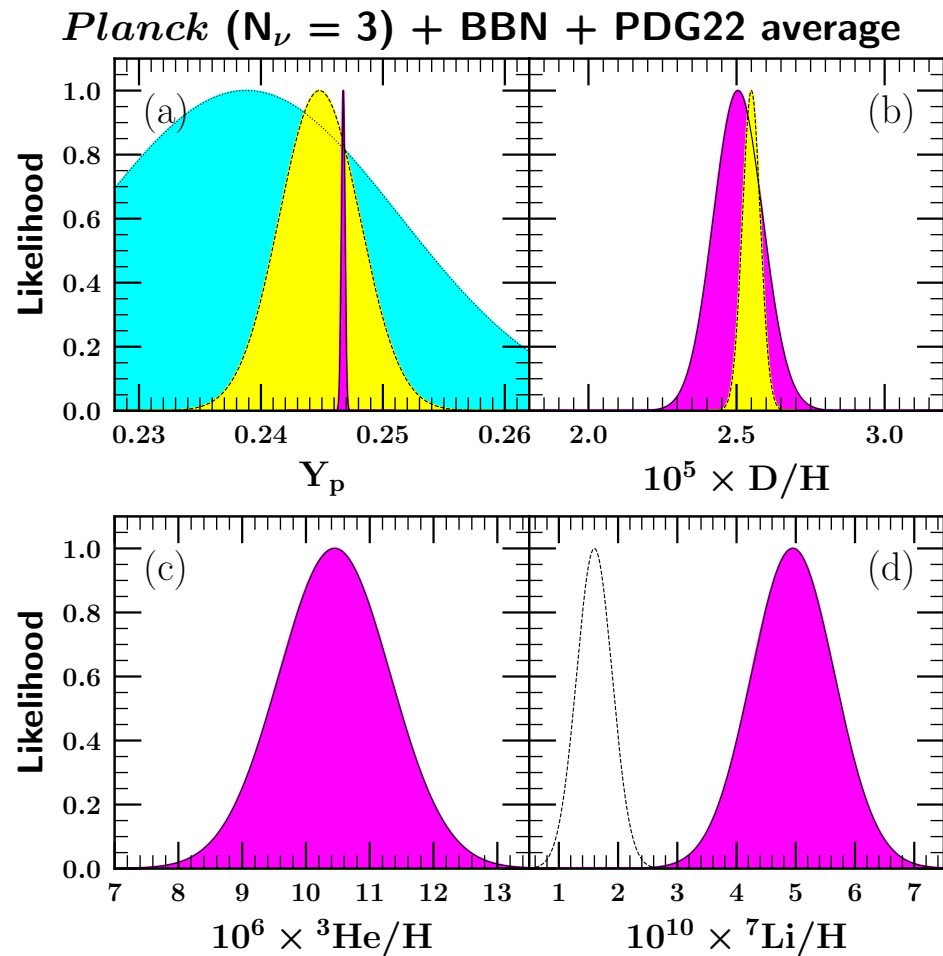
Figure 8. Light element abundance likelihood functions. Shown are the likelihoods for each of the light nuclides: (**a**) the ^{4}He mass fraction, Y_p, (**b**) D/H, (**c**) ^{3}He/H, and (**d**) ^{7}Li. The solid-lined, dark-shaded (purple) curves are the BBN+CMB predictions, based on *Planck* inputs as discussed in the text. The dashed-lined, light-shaded (yellow) curves show astronomical measurements of the primordial abundances, for all but ^{3}He where reliable primordial abundance measures do not exist. For ^{4}He, the dotted-lined, medium-shaded (cyan) curve shows the independent CMB determination of ^{4}He.

In the case of D/H, the observational likelihood is determined from [53–60]

$$\left(\frac{D}{H}\right)_{obs} = (2.55 \pm 0.03) \times 10^{-5}. \tag{21}$$

The agreement between the CMB and BBN likelihoods as seen in panel (b) of Figure 8 is a major success for early Universe cosmology. We have not shown the observational likelihood function for ^{3}He as there are no unambiguous observations that can be associated with the primordial abundance. Similarly, it has been argued that the long-standing problem associated with ^{7}Li [61], is no longer well-founded [62]. The main arguments for associating the observational abundance with the primordial abundance relied on the unambiguous observation of ^{6}Li in halo stars, as well as the lack of dispersion in ^{7}Li abundances at low metallicity. Both of these arguments are now suspect. We show nevertheless, the ^{7}Li abundance from low metallicity by the unshaded likelihood curve at ^{7}Li/H = $(1.6 \pm 0.3) \times 10^{-10}$ [63,64].

The CMB-BBN likelihoods in Figure 8 are summarized by the predicted abundances

$$Y_p \quad = \quad 0.2467 \pm 0.0002 \qquad\qquad (0.2467) \qquad\qquad (22)$$

$$D/H \quad = \quad (2.506 \pm 0.083) \times 10^{-5} \qquad (2.505 \times 10^{-5}) \qquad (23)$$

$$^{3}He/H \quad = \quad (10.45 \pm 0.87) \times 10^{-6} \qquad (10.45 \times 10^{-6}) \qquad (24)$$

$$^{7}Li/H \quad = \quad (4.96 \pm 0.70) \times 10^{-10} \qquad (4.95 \times 10^{-10}) \qquad (25)$$

where the central values give the mean, and the error gives the 1σ variance. The final number in parentheses gives the value at the peak of the distribution.

For comparison, in Figure 9, we also show the same likelihood functions for each of the light elements, but instead, in our Monte Carlo, choose values of the neutron mean life from the ideogram in Figure 3b, rather than the Gaussian distribution. As one can see, apart from the feature on the high side of the BBN ^{4}He distribution (purple shaded likelihood in panel a), the results are very similar, which emphasizes the lack of sensitivity to the current neutron mean life given the experimental uncertainties, even with the dispersion among recent measurements.
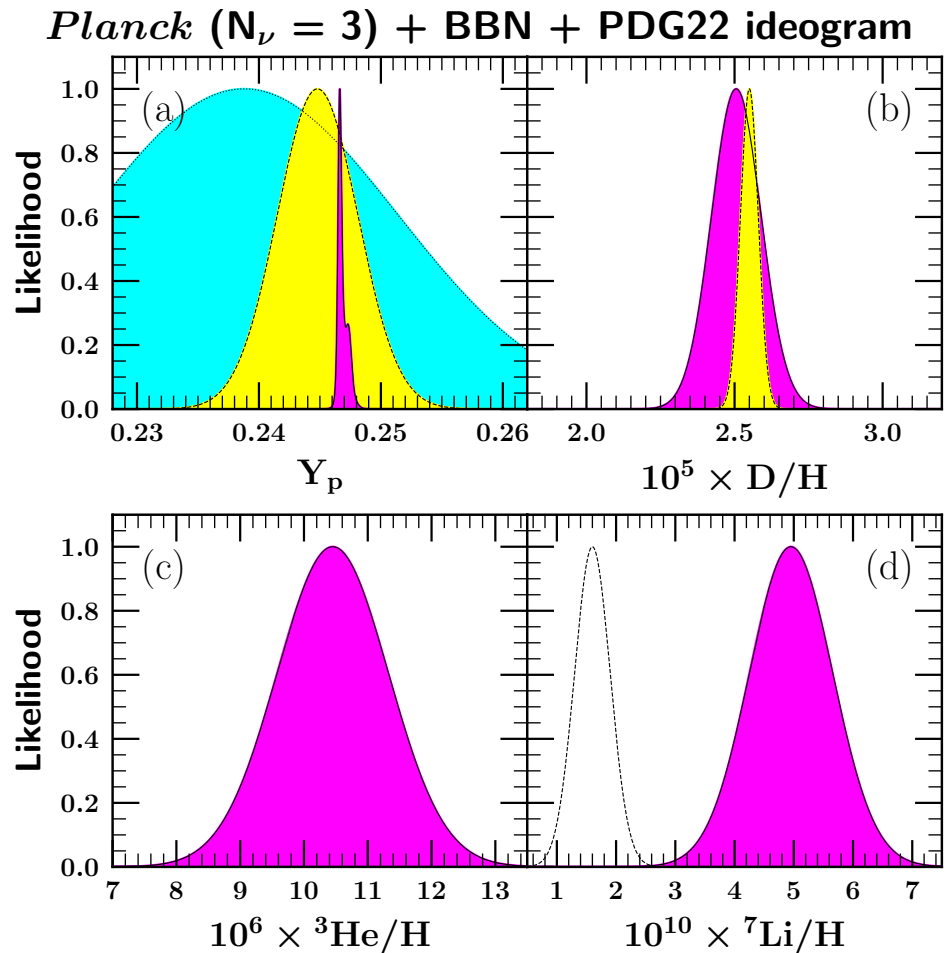
Figure 9. As in Figure 8, where the neutron mean life is selected from the ideogram in Figure 3b rather than the Gaussian distribution.

Similarly, the CMB-BBN likelihoods in Figure 9 using the ideogram in Figure 3b can be summarized by the predicted abundances

$$
\begin{align}
Y_p &= 0.2469 \pm 0.0004 & (0.2466) & \tag{26}\\
\mathrm{D/H} &= (2.507 \pm 0.083) \times 10^{-5} & (2.505 \times 10^{-5}) & \tag{27}\\
{}^3\mathrm{He/H} &= (10.45 \pm 0.87) \times 10^{-6} & (10.45 \times 10^{-6}) & \tag{28}\\
{}^7\mathrm{Li/H} &= (4.96 \pm 0.70) \times 10^{-10} & (4.95 \times 10^{-10})\,. & \tag{29}
\end{align}
$$

The most striking effect between the two distributions is the increase by a factor of 2 in the predicted uncertainty in Y_p.

Finally, we consider the case in which the τ_n errors are dominated by systematics. In this case, it would be inappropriate to use the world average procedure we and the PDG have adopted. Using Equation (1) with $\Delta \tau_n = 5$ s gives $\Delta Y_p = 0.0010 \sim 0.3\sigma_{\mathrm{obs}}(Y_p)$, where $\sigma_{\mathrm{obs}}(Y_p)$ is the observed ^{4}He error in Equation (19). We see that while this shift is large compared to the Y_p theoretical error in Equations (22) and (26), it is small compared to the observed uncertainty. Even if we consider a $\Delta t_n = 10$ s discrepancy between the in-beam measurement and UCNτ trap measurements, the ^{4}He change is $\Delta Y_p = 0.0021 = 0.6\sigma_{\mathrm{obs}}(Y_p)$, and again the shift in the prediction is modest compared to the observed ^{4}He errors. Improvements in the observational ^{4}He abundance are anticipated (see, e.g., [51]), and levels of 0.001 are certainly a goal of future observations. The lesson is that the neutron lifetime does not impact the basic BBN concordance, but also that future improvements in both Y_p and τ_n will make this comparison more interesting, as we now see.

4. BBN 'Predictions' of τ_n

It is also possible to combine the likelihood function in Equation (17) with an observational likelihood function $\mathcal{L}_{\mathrm{OBS}}(Y_p)$ from Equation (19) to obtain a likelihood function for τ_n

$$
\mathcal{L}_{\tau_n}(\tau_n) \propto \int \mathcal{L}_{\mathrm{CMB}}(\eta, Y_p)\, \mathcal{L}_{\mathrm{BBN}}(\eta, \tau_n; Y_p) \mathcal{L}_{\mathrm{OBS}}(Y_p) d\eta\, dY_p\,. \tag{30}
$$

A similar exercise was performed in [65]. This likelihood function (again normalized so that the peak is at $\mathcal{L} = 1$) is shown in Figure 10 by the blue curve. It is characterized by an approximate Gaussian given by

$$
\tau_n(\mathrm{BBN} + \mathrm{CMB}) = 870.2 \pm 15.8 \text{ s} \qquad \text{for } \sigma_{\mathrm{obs}}(Y_p) = 0.0033\,. \tag{31}
$$

Here we use the present $\sigma_{\mathrm{obs}}(Y_p)$ uncertainty as in Equation (19). In Figure 10, we compare this BBN 'prediction' with the Gaussian given by Equation (2) (red dot-dashed curve), and that given by the ideogram (thin cyan curve). We see that the BBN+CMB result is consistent with both the in-beam and trap results for τ_n, but that the errorbars in Equation (31) are too large to discriminate between the shorter and longer experimental measures.

Although we did not discuss it here, the combined BBN and CMB analysis is capable of setting strong constraints on the number of relativistic degrees of freedom at the time of BBN characterized by N_ν. Currently, the joint analysis gives [19] $N_\nu = 2.989 \pm 0.141$ or a 2σ upper limit $N_\nu < 3.180$. The S4 CMB-only sensitivity [66] is expected to reach $\sigma(N_\nu) = 0.07$. That means that if BBN is to remain competitive in the determination of N_ν, improvements in ^{4}He observations are needed so that the uncertainty in Y_p is lowered to 0.001, which is a (perhaps optimistic) goal of the ^{4}He observational program. In that case, we obtain a better determination of τ_n shown by the green dashed curve in Figure 10. In this case, we have

$$
\tau_n(\mathrm{BBN} + \mathrm{CMB}) = 869.8 \pm 4.8 \text{ s} \qquad \text{for } \sigma_{\mathrm{obs}}(Y_p) = 0.001\,. \tag{32}
$$

This can be compared to the likelihood from Equation (2) shown by the dot-dashed red curve. It is no surprise that it will be very difficult for BBN + CMB to compete with direct experimental measurements of the neutron mean life. However, Equation (32) shows that if the ^{4}He observations attain the goal $\sigma_{\mathrm{obs}}(Y_p) = 0.001$, then the BBN+CMB

τ_n prediction will approach the level of the present discrepancy among the experiments, and able to resolve the $\sim$10 s difference between the Yue et al. beam results [43] and the best trap measurements.
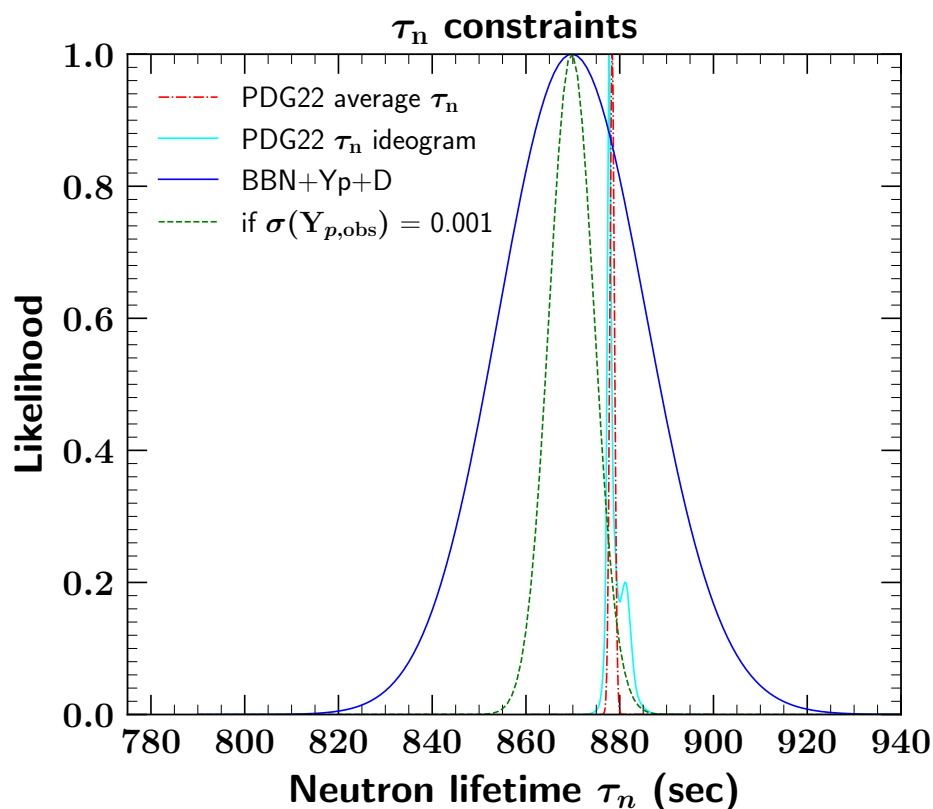
Figure 10. Comparison of the current and potential future BBN predicted likelihood function for τ_n with the experimental likelihood. The solid blue curve shows the current BBN prediction, which is tightened to the green dashed curve if the uncertainty in the helium mass fraction can be reduced to $\sigma_{\mathrm{obs}}(Y_p) = 0.001$. For comparison, the red dot-dashed curve shows the experimental value for τ_n represented by a Gaussian. The distribution represented by the ideogram is shown by the thin cyan solid curve.

5. Summary and Outlook

Motivated by recent interest in the neutron lifetime, we studied the effect of τ_n and its uncertainties on BBN in the post-*Planck* era of precision cosmology. In BBN calculations, the neutron lifetime normalizes the $n \leftrightarrow p$ interconversions before weak freezeout, and then controls free neutron decay. The current discrepancy in neutron lifetime variations thus has an impact on cosmology, which we have assessed.

The continued improvements in τ_n measurements have played a key role in the present robustness and precision of BBN. In the 1980s, the neutron lifetime was a limiting factor in BBN predictions, and it remains the case that the τ_n uncertainty dominates the uncertainty in the ^{4}He predictions. However, as we have shown, modern τ_n data lead to tight predictions of the light element abundances–even given the systematic uncertainties in the neutron lifetime measurements. We showed that combining neutron lifetime measurements as in the PDG ideogram somewhat broadens the errors in the ^{4}He prediction, but this change remains far below the observed ^{4}He errors. Even a $\Delta \tau_n = 10$ s systematic uncertainty would change the Y_p prediction by less than the 1σ uncertainty in the astronomical observations, and the change in the other light elements is negligible. This robustness of the BBN predictions represents a triumph of a nuclear experiment, and allows BBN to play a key role in cosmology and particle physics.

Indeed, the precision of BBN nuclear inputs—and that of CMB observations—allows us to turn the problem around and make a joint BBN+CMB prediction of the neutron lifetime. Our result, $\tau_n(\text{BBN} + \text{CMB}) = 870.2 \pm 15.8$ s (Equation (31)), is consistent within an error range in all experimental determinations. This concordance represents the success of the big bang cosmology, but the agreement arises because the errors in the BBN+CMB predictions are too large (at present) to discriminate among the experiments. We can compare this cosmological measurement of the neutron lifetime with another recent astrophysical determination based on the NASA *Lunar Prospector* measurements of the neutron flux around the Moon: $\tau_n^{\text{Moon}} = 887 \pm 14_{\text{stat}}{}^{+7}_{-3\ \text{syst}}$ s [67]. We see that the two independent results are consistent with errors. We note that, unlike the lunar result, the cosmologically preferred central value lies somewhat below the laboratory results, though the offset is not statistically significant.

Upcoming experiments and observations can improve the current situation and sharpen the link between the neutron lifetime and cosmology. This is important not only for finding the resolution of the τ_n puzzle, but also for BBN. As cosmological measurements become even more precise, it remains important to improve the determination of τ_n and other nuclear inputs to the BBN predictions. We look forward to progress on several fronts.

- New neutron lifetime measurements are planned. These include (a) both an upgrade magneto-gravitational trap experiment UCNτ+, and (b) an upgraded pulsed beam experiment, Beam Lifetime 3 (BL3) [68]. These can shed new light on and perhaps resolve the τ_n puzzle.
- The next generation CMB measurements from CMB-S4 will significantly improve both the determination of Y_p and N_ν from the CMB [66]. Improved τ_n measurements will be important for BBN to fully exploit these results, particularly N_ν.
- The ongoing effort to improve astronomical Y_p determinations continues. As we have discussed here and elsewhere [19], reaching the ambitious goal of $\sigma_{\text{obs}}(Y_p) = 0.001$ would open a new window on new physics generally and τ_n in particular, approaching a precision near that of the present experimental discrepancy.

As these new measurements come in, they will help deepen the links between nuclear physics, particle physics, and early Universe cosmology.

Notes

1.   The arrows at the top of the figure correspond to typical baryon densities taken from mass-to-light ratios typical of the solar neighborhood, the central parts of galaxies, hot gas, and binaries and small groups of galaxies (BSG). At the time, it was not clear what object was truly representative of the cosmological average.

2.   For more information about the construction and use of ideograms, see any issue of the Review of Particle Properties or the Review of Particle Physics.

3.   In fact, we assume ΛCDM, so that in addition to these Standard Model particles and interactions, there is (1) a nonzero cosmological constant Λ which will be negligible during BBN, and (2) cold dark matter which we take to be so weakly interacting as to have no effect on BBN. These assumptions can be relaxed; see reviews in refs. [45–47].

⁴ Including the in-beam measurement would further increase the dispersion requiring a scale factor of 2.2.

References

1. Walker, T.P.; Steigman, G.; Schramm, D.N.; Olive, K.A.; Kang, H.S. Primordial nucleosynthesis redux. *Astrophys. J.* **1991**, *376*, 51–69. [CrossRef]
2. Olive, K.A.; Steigman, G.; Walker, T.P. Primordial nucleosynthesis: Theory and observations. *Phys. Rept.* **2000**, *333*, 389–407. [CrossRef]
3. Fields, B.D.; Olive, K.A. Big bang nucleosynthesis. *Nucl. Phys.* **2006**, *777*, 208–225. [CrossRef]
4. Fields, B.D.; Molaro, P.; Sarkar, S. Big-Bang Nucleosynthesis. *Chin. Phys. C* **2014**, *38*, 339–344. [CrossRef]
5. Steigman, G. Primordial Nucleosynthesis in the Precision Cosmology Era. *Ann. Rev. Nucl. Part. Sci.* **2007**, *57*, 463–491. [CrossRef]
6. Iocco, F.; Mangano, G.; Miele, G.; Pisanti, O.; Serpico, P.D. Primordial Nucleosynthesis: From precision cosmology to fundamental physics. *Phys. Rep.* **2009**, *472*, 1–76. [CrossRef]
7. Pitrou, C.; Coc, A.; Uzan, J.P.; Vangioni, E. Precision big bang nucleosynthesis with improved Helium-4 predictions. *Phys. Rep.* **2018**, *754*, 1–66. [CrossRef]
8. Cyburt, R.H.; Fields, B.D.; Olive, K.A.; Yeh, T.-H. Big Bang Nucleosynthesis: 2015. *Rev. Mod. Phys.* **2016**, *88*, 015004. [CrossRef]
9. Fields, B.D.; Olive, K.A.; Yeh, T.H.; Young, C. Big-Bang Nucleosynthesis after Planck. *J. Cosmol. Astropart. Phys.* **2020**, *3*, 010. [CrossRef]
10. Particle Data Group; Workman, R.L.; Burkert, V.D.; Crede, V.; Klempt, E.; Thoma, U.; Tiator, L.; Agashe, K.; Aielli, G.; Allanach, B.C.; et al. Review of Particle Physics. *Prog. Theor. Exp. Phys.* **2022**, *2022*, 083C01.
11. Aghanim, N.; Akrami, Y.; Ashdown, M.; Aumont, J.; Baccigalupi, C.; Ballardini, M.; Barreiro, R.B.; Bartolo, N.; Basak, S.; Battye, R. Planck 2018 results. VI. Cosmological parameters. *Astron. Astrophys.* **2020**, *641*, A6.
12. Janot, P.; Jadach, S. Improved Bhabha cross section at LEP and the number of light neutrino species. *Phys. Lett. B* **2020**, *803*, 135319. [CrossRef]
13. Olive, K.A.; Schramm, D.N.; Steigman, G.; Turner, M.S.; Yang, J.M. Big Bang Nucleosynthesis as a Probe of Cosmology and Particle Physics. *Astrophys. J.* **1981**, *246*, 557. [CrossRef]
14. Yang, J.M.; Turner, M.S.; Steigman, G.; Schramm, D.N.; Olive, K.A. Primordial Nucleosynthesis: A Critical Comparison of Theory and Observation. *Astrophys. J.* **1984**, *281*, 493–511. [CrossRef]
15. Ellis, J.R.; Olive, K.A. Constraints on Light Particles From Stellar Evolution. *Nucl. Phys. B* **1983**, *223*, 252–268. [CrossRef]
16. Christensen, C.J.; Nielsen, A.; Bahnsen, A.; Brown, W.K.; Rustad, B.M. Free-Neutron Beta-Decay Half-Life. *Phys. Rev. D* **1972**, *5*, 1628–1640. [CrossRef]
17. Bondarenko, L.N.; Kurguzov, V.V.; Prokofev, Y.A.; Rogov, E.V.; Spivak, P.E. Measurement of the Neutron Half Time. *Pisma Zh. Eksp. Teor. Fiz.* **1978**, *28*, 328–333.
18. Byrne, J.; Morse, J.; Smith, K.F.; Shaikh, F.; Green, K.; Greene, G.L. A New Measurement of the Neutron Lifetime. *Phys. Lett. B* **1980**, *92*, 274–278. [CrossRef]
19. Yeh, T.H.; Shelton, J.; Olive, K.A.; Fields, B.D. Probing physics beyond the standard model: Limits from BBN and the CMB independently and combined. *J. Cosmol. Astropart. Phys.* **2022**, *10*, 046. [CrossRef]
20. Baltrusaitis, R.M.; Becker, J.; Blaylock, G.; Brown, J.S.; Bunnell, K.; Burnett, T.; Cassell, R.; Coffman, D.; Cook, V.; Coward, D.H.; et al. [Particle Data Group]. Decays of the J/ψ into Two Pseudoscalar Mesons. *Phys. Lett. B* **1982**, *111*, 1–294.
21. Kosvintsev, Y.Y.; Kushnir, Y.A.; Morozov, V.I.; Terekhov, G.I. Application of Ultracold Neutrons for Neutron Lifetime Measurement. *JETP Lett.* **1980**, *31*, 236. (In Russian)
22. Wilkinson, D.H. The neutron lifetime. *Prog. Part. Nucl. Phys.* **1981**, *6*, 325–332. [CrossRef]
23. Tanabashi, M.; Hagiwara, K.; Hikasa, K.; Nakamura, K.; Sumino, Y.; Takahashi, F.; Tanaka, J.; Agashe, K.; Aielli, G.; Amsler, C.; et al. Review of Particle Properties. Particle Data Group. *Rev. Mod. Phys.* **1984**, *56*, S1–S304.
24. Mampe, W.; Ageron, P.; Bates, C.; Pendlebury, J.M.; Steyerl, A. Neutron Lifetime Measured With Stored Ultracold Neutrons. *Phys. Rev. Lett.* **1989**, *63*, 593–596. [CrossRef]
25. Olive, K.A.; Schramm, D.N.; Steigman, G.; Walker, T.P. Big Bang Nucleosynthesis Revisited. *Phys. Lett. B* **1990**, *236*, 454–460. [CrossRef]
26. Yeh, T.H.; Olive, K.A.; Fields, B.D. The impact of new $d(p, \gamma)3$ rates on Big Bang Nucleosynthesis. *J. Cosmol. Astropart. Phys.* **2021**, *3*, 046. [CrossRef]
27. Hagiwara, K. Review of Particle Physics. *Phys. Rev. D* **2002**, *66*, 010001. [CrossRef]
28. Arzumanov, S.; Bondarenko, L.; Chernavsky, S.; Fomin, A.; Morozov, V.; Panin, Y.; Drexel, W.; Schreckenbach, K.; Geltenbort, P.; Pendlebury, J. Neutron life time value measured by storing ultracold neutrons with detection of inelastically scattered neutrons. *Phys. Lett. B* **2000**, *483*, 15–22. [CrossRef]
29. Cyburt, R.H.; Fields, B.D.; Olive, K.A. The NACRE Thermonuclear Reaction Compilation and Big Bang Nucleosynthesis. *New Astron.* **1996**, *6*, 215. [CrossRef]
30. Spergel, D.N.; Verde, L.; Peiris, H.V.; Komatsu, E.; Nolta, M.R.; Bennett, C.L.; Halpern, M.; Hinshaw, G.; Jarosik, N.; Kogut, A.; et al. First year Wilkinson Microwave Anisotropy Probe (WMAP) observations: Determination of cosmological parameters. *Astrophys. J. Suppl.* **2003**, *148*, 175–194. [CrossRef]

31. Cyburt, R.H.; Fields, B.D.; Olive, K.A. Primordial nucleosynthesis with CMB inputs: Probing the early universe and light element astrophysics. *Astropart. Phys.* **2002**, *17*, 87–100. [CrossRef]

32. Serebrov, A.; Varlamov, V.; Kharitonov, A.; Fomin, A.; Pokotilovski, Y.; Geltenbort, P.; Butterworth, J.; Krasnoschekova, I.; Lasakov, M.; Tal'daev, R.; et al. Measurement of the neutron lifetime using a gravitational trap and a low-temperature Fomblin coating. *Phys. Lett. B* **2005**, *605*, 72–78. [CrossRef]

33. Mathews, G.J.; Kajino, T.; Shima, T. Big Bang nucleosynthesis with a new neutron lifetime. *Phys. Rev. D* **2005**, *71*, 021302. [CrossRef]

34. Beringer, J.; Arguin, J.F.; Barnett, R.M.; Copic, K.; Dahl, O.; Groom, D.E.; Lin, C.J.; Lys, J.; Murayama, H.; Wohl, C.G.; et al. [Particle Data Group]. Review of Particle Physics (RPP). *Phys. Rev. D* **2012**, *86*, 010001. [CrossRef]

35. Wietfeldt, F.E.; Greene, G.L. Colloquium: The neutron lifetime. *Rev. Mod. Phys.* **2011**, *83*, 1173–1192. [CrossRef]

36. Pichlmaier, A.; Varlamov, V.; Schreckenbach, K.; Geltenbort, P. Neutron lifetime measurement with the UCN trap-in-trap MAMBO II. *Phys. Lett. B* **2010**, *693*, 221–226. [CrossRef]

37. Steyerl, A.; Pendlebury, J.M.; Kaufman, C.; Malik, S.S.; Desai, A.M. Quasielastic scattering in the interaction of ultracold neutrons with a liquid wall and application in a reanalysis of the Mambo I neutron-lifetime experiment. *Phys. Rev. C* **2012**, *85*, 065503. [CrossRef]

38. Arzumanov, S.; Bondarenko, L.; Chernyavsky, S.; Geltenbort, P.; Morozov, V.; Nesvizhevsky, V.V.; Panin, Y.; Strepetov, A. A measurement of the neutron lifetime using the method of storage of ultracold neutrons and detection of inelastically up-scattered neutrons. *Phys. Lett. B* **2015**, *745*, 79–89. [CrossRef]

39. Serebrov, A.P.; Kolomensky, E.A.; Fomin, A.K.; Krasnoshchekova, I.A.; Vassiljev, A.V.; Prudnikov, D.M.; Shoka, I.V.; Chechkin, A.V.; Chaikovskiy, M.E.; Varlamov, V.E.; et al. Neutron lifetime measurements with a large gravitational trap for ultracold neutrons. *Phys. Rev. C* **2018**, *97*, 055503. [CrossRef]

40. Pattie, R.W., Jr.; Callahan, N.B.; Cude-Woods, C.; Adamek, E.R.; Broussard, L.J.; Clayton, S.M.; Currie, S.A.; Dees, E.B.; Ding, X.; Engel, E.M.; et al. Measurement of the neutron lifetime using a magneto-gravitational trap and in situ detection. *Science* **2018**, *360*, 627–632. [CrossRef]

41. Ezhov, V.F.; Andreev, A.Z.; Ban, G.; Bazarov, B.A.; Geltenbort, P.; Glushkov, A.G.; Knyazkov, V.A.; Kovrizhnykh, N.A.; Krygin, G.B.; Naviliat-Cuncic, O.; et al. Measurement of the neutron lifetime with ultra-cold neutrons stored in a magneto-gravitational trap. *JETP Lett.* **2018**, *107*, 671–675. [CrossRef]

42. Gonzalez, F.M.; Fries, E.M.; Cude-Woods, C.; Bailey, T.; Blatnik, M.; Broussard, L.J.; Callahan, N.B.; Choi, J.H.; Clayton, S.M.; Currie, S.A.; et al. Improved neutron lifetime measurement with UCNτ. *Phys. Rev. Lett.* **2021**, *127*, 162501. [CrossRef] [PubMed]

43. Yue, A.T.; Dewey, M.S.; Gilliam, D.M.; Greene, G.L.; Laptev, A.B.; Nico, J.S.; Snow, W.M.; Wietfeldt, F.E. Improved Determination of the Neutron Lifetime. *Phys. Rev. Lett.* **2013**, *111*, 222501. [CrossRef] [PubMed]

44. Czarnecki, A.; Marciano, W.J.; Sirlin, A. Neutron Lifetime and Axial Coupling Connection. *Phys. Rev. Lett.* **2018**, *120*, 202002. [CrossRef] [PubMed]

45. Pospelov, M.; Pradler, J. Big Bang Nucleosynthesis as a Probe of New Physics. *Ann. Rev. Nucl. Part. Sci.* **2010**, *60*, 539–568. [CrossRef]

46. Jedamzik, K.; Pospelov, M. Big Bang Nucleosynthesis and Particle Dark Matter. *New J. Phys.* **2009**, *11*, 105028. [CrossRef]

47. Malaney, R.A.; Mathews, G.J. Probing the early universe: A Review of primordial nucleosynthesis beyond the standard Big Bang. *Phys. Rept.* **1993**, *229*, 145–219. [CrossRef]

48. Bernstein, J.; Brown, L.S.; Feinberg, G. Cosmological Helium Production Simplified. *Rev. Mod. Phys.* **1989**, *61*, 25. [CrossRef]

49. Mukhanov, V.F. Nucleosynthesis without a computer. *Int. J. Theor. Phys.* **2004**, *43*, 669. [CrossRef]

50. Froustey, J.; Pitrou, C. Incomplete neutrino decoupling effect on big bang nucleosynthesis. *Phys. Rev. D* **2020**, *101*, 043524. [CrossRef]

51. Aver, E.; Berg, D.A.; Olive, K.A.; Pogge, R.W.; Salzer, J.J.; Skillman, E.D. Improving helium abundance determinations with Leo P as a case study. *J. Cosmol. Astropart. Phys.* **2021**, *3*, 027. [CrossRef]

52. Aver, E.; Berg, D.A.; Hirschauer, A.S.; Olive, K.A.; Pogge, R.W.; Rogers, N.S.J.; Salzer, J.J.; Skillman, E.D. A comprehensive chemical abundance analysis of the extremely metal poor Leoncino Dwarf galaxy (AGC 198691). *Mon. Not. R. Astron. Soc.* **2021**, *510*, 373–382. [CrossRef]

53. Pettini, M.; Cooke, R. A new, precise measurement of the primordial abundance of Deuterium. *Mon. Not. R. Astron. Soc.* **2012**, *425*, 2477–2486. [CrossRef]

54. Cooke, R.; Pettini, M.; Jorgenson, R.A.; Murphy, M.T.; Steidel, C.C. Precision measures of the primordial abundance of deuterium. *Astrophys. J.* **2014**, *781*, 31. [CrossRef]

55. Riemer-Sørensen, S.; Webb, J.K.; Crighton, N.; Dumont, V.; Ali, K.; Kotuš, S.; Bainbridge, M.; Murphy, M.T.; Carswell, R. A robust deuterium abundance; Re-measurement of the z = 3.256 absorption system towards the quasar PKS1937-1009. *Mon. Not. R. Astron. Soc.* **2015**, *447*, 2925–2936. [CrossRef]

56. Balashev, S.A.; Zavarygin, E.O.; Ivanchik, A.V.; Telikova, K.N.; Varshalovich, D.A. The primordial deuterium abundance: SubDLA system at $z_{abs} = 2.437$ towards the QSO J 1444+2919. *Mon. Not. R. Astron. Soc.* **2016**, *458*, 2188–2198. [CrossRef]

57. Cooke, R.J.; Pettini, M.; Nollett, K.M.; Jorgenson, R. The primordial deuterium abundance of the most metal-poor damped Lyα system. *Astrophys. J.* **2016**, *830*, 148. [CrossRef]

58. Riemer-Sørensen, S.; Kotuš, S.; Webb, J.K.; Ali, K.; Dumont, V.; Murphy, M.T.; Carswell, R.F. A precise deuterium abundance: Remeasurement of the z = 3.572 absorption system towards the quasar PKS1937?101. *Mon. Not. R. Astron. Soc.* **2017**, *468*, 3239–3250. [CrossRef]

59. Zavarygin, E.O.; Webb, J.K.; Dumont, V.; Riemer-Sørensen, S. The primordial deuterium abundance at z_{abs} = 2.504 from a high signal-to-noise spectrum of Q1009 + 2956. *Mon. Not. R. Astron. Soc.* **2018**, *477*, 5536–5553. [CrossRef]

60. Cooke, R.J.; Pettini, M.; Steidel, C.C. One Percent Determination of the Primordial Deuterium Abundance. *Astrophys. J.* **2018**, *855*, 102. [CrossRef]

61. Cyburt, R.H.; Fields, B.D.; Olive, K.A. An Update on the big bang nucleosynthesis prediction for Li-7: The problem worsens. *J. Cosmol. Astropart. Phys.* **2008**, *11*, 012. [CrossRef]

62. Fields, B.D.; Olive, K.A. Implications of the non-observation of ^{6}Li in halo stars for the primordial ^{7}Li problem. *J. Cosmol. Astropart. Phys.* **2022**, *10*, 078. [CrossRef]

63. Ryan, S.G.; Beers, T.C.; Olive, K.A.; Fields, B.D.; Norris, J.E. Primordial Lithium and Big Bang Nucleosynthesis. *Astrophys. J.* **2000**, *530*, L57. [CrossRef]

64. Sbordone, L.; Bonifacio, P.; Caffau, E.; Ludwig, H.-G.; Behara, N.T.; Hernandez, J.I.G.; Steffen, M.; Cayrel, R.; Freytag, B.; Van't Veer, C. et al. The metal-poor end of the Spite plateau. 1: Stellar parameters, metallicities and lithium abundances. *Astron. Astrophys.* **2010**, *522*, A26. [CrossRef]

65. Salvati, L.; Pagano, L.; Consiglio, R.; Melchiorri, A. Cosmological constraints on the neutron lifetime. *J. Cosmol. Astropart. Phys.* **2016**, *3*, 055. [CrossRef]

66. Abazajian, K.N.; Adshead, P.; Ahmed, Z.; Allen, S.W.; Alonso, D.; Arnold, K.S.; Baccigalupi, C.; Bartlett, J.G.; Battaglia, N.; Benson, B.A.; et al. CMB-S4 Science Book, First Edition. *arXiv* **2016**, arXiv:1610.02743.

67. Wilson, J.T.; Lawrence, D.J.; Peplowski, P.N.; Eke, V.R.; Kegerreis, J.A. Measurement of the free neutron lifetime using the neutron spectrometer on NASA's Lunar Prospector mission. *Phys. Rev. C* **2021**, *104*, 045501. [CrossRef]

68. Wietfeldt, F.E.; Biswas, R.; Caylor, J.; Crawford, B.; Dewey, M.S.; Fomin, N.; Greene, G.L.; Haddock, C.C.; Hoogerheide, S.F.; Mumm, H.P.; et al. Comments on Systematic Effects in the NIST Beam Neutron Lifetime Experiment. *arXiv* **2022**, arXiv:2209.15049.